Al-Azhar Bulletin of Science

Volume 29 | Issue 2 Article 30

12-1-2018
Section: Chemistry

THE ADSORPTION KINETICS AND MODELING FOR Pb(II) REMOVAL FROM SYNTHETIC AND REAL WASTEWATER BY MORINGA OLEIFERA SEEDS

A. Swelam
Faculty of Science, chemistry Dept. Al Azhar University, Egypt

S. Sherif
Medicinal and Aromatic Dept. Horti. Res. Institute, A. R. C., Egypt

A. Ibrahim
Faculty of Science, chemistry Dept. Al Azhar University, Egypt

How to Cite This Article

Swelam, A.; Sherif, S.; and Ibrahim, A. (2018) "THE ADSORPTION KINETICS AND MODELING FOR Pb(II) REMOVAL FROM SYNTHETIC AND REAL WASTEWATER BY MORINGA OLEIFERA SEEDS," *Al-Azhar Bulletin of Science*: Vol. 29: Iss. 2, Article 30.
DOI: https://doi.org/10.21608/absb.2018.33773

Al Azhar Bulletin of Science Vol. 29, No. 2 (December), 2018, pp. 105-124

THE ADSORPTION KINETICS AND MODELING FOR Pb(II) REMOVAL FROM SYNTHETIC AND REAL WASTEWATER BY MORINGA OLEIFERA SEEDS

A.A.Swelam[1], S.S.Sherif[2] and A.Ibrahim[3].

[1,3] *Faculty of Science, chemistry Dept. Al Azhar University, Egypt*
[2] *Medicinal and Aromatic Dept. Horti. Res. Institute, A. R. C., Egypt*

ABSTRACT

This work demonstrates the potential of Moringa oleifera seeds powder as an adsorbent for the removal of heavy metals from wastewater. The moringa oleifera seeds powder is characterized as an adsorbent for the removal of heavy metals from wastewater using FTIR, XRD, pH_{pzc}, SEM and BET techniques. Several processing parameters such as; contact time, adsorbent dose, initial lead ion concentrations, pH, and temperature are optimized. The equilibrium data for bio-sorption are analyzed by using Langmuir, Freundlich, Temkin and Dubinin–Radushkevich isotherm models to define the best correlation for lead ions. Among the four isotherm models, both Temkin and Freundlich models best describe the experimental data for Pb(II).The adsorption of the metal ions, Pb (II) is well defined by the pseudo-second order model ($R^2 > 0.99$). The interaction of the cationic species with the MOS powder is predominately via chemisorption rather than physisorption. The thermodynamic parameters such as ΔS, ΔH and ΔG are also determined.

Key words: Moringa oleifera seeds, pb(II), adsorption, removal, kinetics.

INTRODUCTION

Heavy metals have hazardous impact to ecosystem including human, animals and plant health. Therefore, the Word Heath Organization (WHO) and Environmental Protection Agency (EPA) have regulated the maximum acceptable discharge level into the environments and thus controlling the water pollution level. According to U.S. Environmental Protection Agency (EPA), Agency for Toxic Substances and Disease Registry (ATSDR), and World Health Organization (WHO), the max acceptable concentrations recommended for zinc, copper, chromium and nickel in drinking water is 3.00, 2.00, 0.05 and 0.02 mg/L, respectively [1].Lead (Pb^{2+}) is an ubiquitous toxic heavy metal in the environment [2]. Pb^{2+}toxicitiesoccur when organisms, especially during their infancy, inhale or ingest a concentrated source of Pb^{2+}. In humans, Pb^{2+} toxicity causes neurological and hematological dysfunctions, hepatic and renal damage and reproductive disorders [3]. Generally, humans are exposed to Pb^{2+} primarily via the food chain because some vegetables, grains and fruits may be unknowingly grown in Pb-contaminated soil or may be irrigated with Pb^{2+}-contaminated water. Similarly, animal products can also be contaminated with heavy metals such as Pb^{2+}[4].Bio-sorption represents the ability of biological materials in removal of heavy metals from aqueous effluents. Bio-sorbents have high efficiency, selectivity and its natural affinity to metal ions. The mechanism of removal can be described as ion exchange, electrostatic force and precipitation. In addition, bio-sorption is widely used due to their natural availability in environment and low costs.

Vieira et al. [5] showed that MO seeds used as a natural adsorbent have a strong removal efficiency reaching up to 98% for both color and turbidity. While **Arnoldsson et al**. [6] mentioned the negligible effect of MO seeds as a coagulant on pH, alkalinity or conductivity of water. MO seeds have not only been studied for their coagulating properties but also for their ability to remove heavy metals from aqueous solutions. A study by **Nand et al.** [7] showed that MO was capable on adsorbing heavy metals more than other seed types. The percentage of removal was 90% for copper, 80% for lead, 60% for cadmium and 50% for zinc and chromium.

Accordingly, the goal of this work is to systematically evaluate the removal characteristics of high concentration lead by

moringa oleifera seed (MOS). The specific objects of this study are to (1) investigate the effects of different factors such as MOS dosage, lead concentrations, contact time, solution pH, temperature and agitation time, on lead removal; (2) simulate the equilibrium adsorption data with different isotherm models such as Langmuir, Freundlich, Temkin and Dubinin–Radushkevich, and identify the equilibrium adsorption model of lead on MOS; (3) analyze the kinetic data (Pseudo-first order Pseudo-second order and Elovich models) and interpret the kinetics process of lead adsorption on MOS The characterization of the Adsorbent was made using (FTIR), SEM, EDX, X-ray, and point of zero charge (pH_{pzc}).

2- EXPERIMENTAL

Materials

Synthetic wastewater solutions are prepared by dissolving a desired amount of lead acetate (g) of analytical grade in distilled water to obtain stock solution. All the chemicals used are of analytical grade. Distilled water is used throughout the experiments.

Instrumentation

Identification of the various functional groups of the moringa oleifera seed powder is accomplished using a KBr pellets and analyzed with a Shimadzu FTIR spectrometer (model 8201PC). The spectra are recorded in the absorption band mode, in the 4000-400 cm^{-1} range (Central lab of faculty of science–Ain shams university, Cairo, Egypt). A Perkin Elmer, Analyst 400, Flame Atomic Absorption Spectrometry (National Research center–Giza–Egypt). The pH of the solution is determined using a HANNA instruments pH meter (pH 209 models, Portugal). X-ray diffraction measurements are done using a high resolution. The XRD measurements are done using a Bruker D8 Discover (Cu Kα radiation at 40 kV and 40 mA) with a GADDS-detector system(V˚ANTEC-500) (Egypt Nanotechnology Center, Cairo University, Shaikh Zayed Campus, B3). The surface morphology is studied using a Jeol (Tokyo , Japan) JSM 5600 LV. Oxford instruments 6587 EDX micro-analysis detector EDX micro-analysis is made to obtain information on the elemental composition of the sample (Egypt Nanotechnology Center, Cairo University, Shaikh Zayed Campus, B3). A micrometrics(Nova touch LX2, Quanta chrome Instruments, Boynton Beach, Florida, USA (Egypt Nanotechnology Center, Cairo University, Shaikh Zayed Campus, B3 instrument) is used for Brunau-Emmett-Teller (BET) analysis to determine information such as surface area, total pore volume, and average pore size of moringa seed powder. In a BET surface area analysis, a dry sample is evacuated of all gas and cooled to 77˚K using liquid nitrogen.

Moringa oleifera seeds

M. oleifera seeds (MOS) are obtained from Al Qalyobia Farm (Medicinal and Aromatic Dept., Horticulture Res. Institute, A.R.C., Egypt) December in 2016. The seeds are identified by the Horticulture Research Institute of Egypt. Seeds was de-shelled by hand, dried and then grounded in a domestic blender and sieved through 0.08 mm stainless steel sieve

Batch adsorption experimental procedures

The batch experiment is carried out by firstly weighing 0.666 g of dried and sieved powered seeds. A desired amount of the stock lead solution is added and the mixture shaken in a mechanical shaker at 100 rpm for a definite period of time (5–300 min) until equilibrium is reached. The metal ions are further analyzed with atomic adsorption spectroscopy. The experiments are carried out in three times and mean values are taken for calculation. The adsorption efficiency (%) is calculated according to the expressions:

$$\% \text{ Adsorption} = (C_o - C_e) \times 100/C_0 \quad (1)$$

The adsorption capacity at equilibrium, q_e (mg/g), of the metals were calculated using equation (2);

$$q_e = V(C_o - C_e)/W \times 1000 \quad (2)$$

where, C_o and Ce (mg/L) are the liquid-phase concentrations of Pd(II) at time zero and equilibrium, respectively. V is the volume (L) of the sample solution and W is the weight (g) of the dry sorbent.

3- RESULTS AND DISCUSSION

Characterization of Moringa Oleifera Seed powder

Fourier transforms infrared (FTIR) spectroscopy

It is very crucial to elucidate the functional groups in order to understand the interaction between the adsorbent and the metal ion. The Fourier Transform Infrared (FT-IR) spectra (Fig. 1) of MOS (unloaded) and metal-loaded MOS are recorded at 400–4000 cm^{-1} range using an FT-IR to investigate the functional groups present on the bio-sorbent surface.

The bands in approximately 2924.8 cm^{-1} and 2854.1 cm^{-1} are assigned to the symmetric and asymmetric stretching of group C-H-CH_2 present in fatty acids [8]. The spectra showed two strong absorption bands at 1657.5 $cm^{-1}$and a 1543.7 cm^{-1} characteristics of amide I and II respectively, which confirms the structure of the protein present in Moringa seeds and is approximately 1114.4 cm^{-1}, concerning the presence of polysaccharides [9]. Thus, in general, the FTIR's spectra of moringa oleifera seed showed the presence of various functional groups, indicating in this way their complex nature. The peak at 1746 cm^{-1} in the MOS spectrum shows the carbonyl (C=O) stretching vibration of the carboxyl groups of lignin in the MO [10]. The broad peak in spectra at 3313.1 cm^{-1} is indicative of strong O-H (H-bonded) stretching [11]. As can be observed from Fig. 1 referring to MOS as the substrate for adsorption, the peaks in both the spectra obtained before and after adsorption displayed characteristic bands at 870.4, 789.6 and 461.8 cm^{-1} for the raw MOS, bands at 851.2, 582.2 and 462.3 cm^{-1} for adsorption of lead ions which can be attributed to Si-O stretching modes and Si-O-Si bending modes including distortion modes associated primarily with oxygen and silica atoms respectively [12] and bands at 1096.9, 852.3 and 463.1 cm^{-1} for adsorption of lead ions.

In this work, it is observed that the Moringa olefira seed has amide, amine, carboxylic acid, hydroxyl and other functional groups, which possibly confirmed the presence of most of the necessary functionalities in the current study. A similar type of Moringa seed spectra has also been reported by other scientists, during different research findings [13,14]. Comparison of the FTIR spectra of the MOS before and after adsorption of the metal ions revealed that, after adsorption of Pb(II), the peaks are shifted significantly or not changed (Fig. 1). The shifting in the peak positions and intensity in the spectra, after Pb(II) adsorption, signifies the participation of those specific groups in sorption process. So the functional groups like O-H, C-N, N-H and C-O are possibly playing their role in sorption phenomenon by developing some electrostatic forces or complexion [15] between the functional groups on bio-sorbent surfaces and the metal ions. In addition, there is a need to perform structural studies under the conditions in which protein actually operates (i.e. generally in solution).

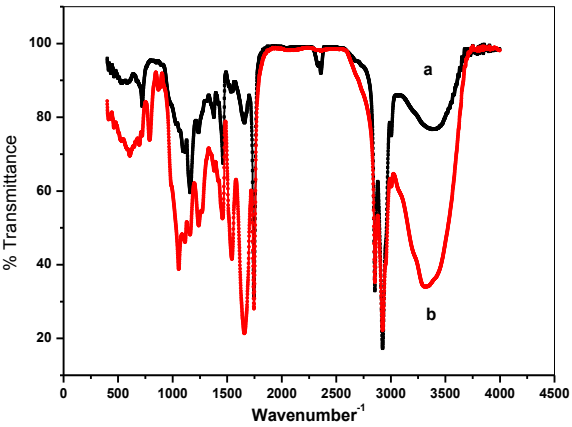

Fig.1. FT-IR diffraction of Moringa Oleifera seed before (a) and after (b) Pb(II) adsorption

Thus, further investigations are necessary to study the infrared spectra of the adsorbent protein in aqueous solution. The change in the positions of the groups confirmed their role in the ion binding to the MOS surface [16,17].

XRD studies

A powerful tool for showing the crystalline and amorphous region is XRD spectroscopy. The XRD patterns of MOS and MOS-Pb systems.

Fig. 2 show the X-ray diffraction pattern of moringa oleifera seed powder. According to **Abudikarim et al.** [18], around 69% weight of

the seeds composed of high amount of oil and protein. Due to the high composition of protein and oil, the X-ray pattern showed a broad band around $2\Theta = 20°$ for the seed powder which is attributed to the predominance of amorphous nature of the material. The presence of this peak is probably associated with diffraction of the constituent protein surrounding the other components that have a more amorphous or semi crystalline nature [14]. According to **Araújo et al. 2013** and **Isabela et al., 2018** [19,20], the amorphous nature of the adsorbent suggests that the adsorbate can more easily penetrate the surface of the adsorbent, thus favoring the adsorption process.A noticeable change in the X-ray diffraction (XRD) peak positions is observed due to the addition of Pb(II) ions. Therefore, it is concluded that the incorporation of the ions in the MOS affects the amorphous surface of the MOS, thus increasing crystalline structure . This is due to the fact that the replacement of protons of hydroxyl and carboxylic groups presented on the MOS surface, thus the adsorption of these ions is partially via ion exchange mechanism**.** This then explains the formation of new peaks, disappearance of others and band shifts observed on the water-soluble protein powder after removal.

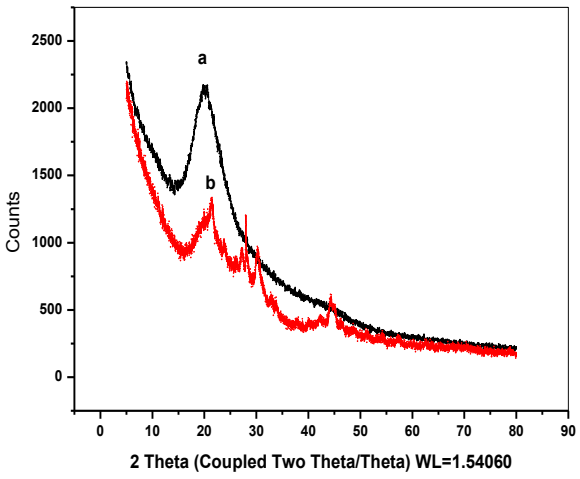

Fig.2. XRD of Moringa Oleifera seed before (a) and after (b) Pb(II) adsorption

Pore structure analysis

The pore characteristics of the moringa oleifera seed mainly depend on the raw materials conditions. The prepared MOS had a surface area of 20.4091 m^2/g, a total pore volume of 0.0167454 cc/g, average pore size 1.64098 nm(Microporous< 2 nm). Moreover, the average pore size (1.64098 nm< 2 nm) confirmed the micro porous structure of the MOS, which favored the adsorption of low-to medium-sized molecules [18,21]. In general, natural materials with small surface areas are expected, as in the case of moringa seeds, and therefore the functional groups present on their surfaces characterize the adsorption capacity.

A scanning electron microscope (SEM)

Fig. 3 shows SEM images of the moringa oleifera seeds used to analyze the morphologies of the studied adsorbent. Fig. 3 shows that the material formed by MOS are both spherical and villous, moreover, the villus is presented as Nano scale. The villous structure covered on the MOS was much thin. It can be speculated that the spherical structure and Nano scale villus plays an important role in the adsorption process [22]. It is observed also that, the material exhibit a heterogeneous and relatively porous matrix. The spaces available facilitate the adsorption process because they provide a high internal surface area. The same conclusion was reported by **Araújo et al. 2010**[8]. The author also explains that this structure facilitates the ionic adsorption processes due to the interstices and, more importantly, the presence of the protein component of the seed. The porous nature of this material can also be observed in the data obtained with the BET analysis. The results also indicate that, there was a layer covering the surfaces of the Moringa oleifera seed, possibly lead (Fig.3). A similar type of other adsorbent spectra has also been reported by other scientists, during different research findings [23,24].

To further confirm the role of the localized elemental information of MOS, the EDX study was determined, which presented the important elements of the MOS adsorbent (Fig. 4). Fig. 4 show the EDS patterns of MOS adsorbent before and after adsorption. The oxygen, nitrogen and silicon element occurs at the surface, which are favorable for the adsorption of heavy metal ions. The presence of C is also associated with the high protein content in MO

seeds [25] which contributes to the efficiency of this material in the adsorption process. Based on the results of Fig. 4, it can be found that the elements of O, N and Si are significantly reduced after adsorption while the Pb(II) ions peaks are appeared. The reduction of these ions may be contribution of ion exchange reaction with heavy metal ions Pb(II) in the adsorption process. Consequently, it can be summarized that the surface oxygen-containing functional groups and other metal ions of adsorbent have a significant role in the adsorption process.

The pH of zero point charges (pH_{PZC}) of the MOS

Surface charge of the sorbent play a major role in the sorption systems .The pH of zero point charges (pH_{PZC}) of the moringa oleifera seed (MOS) is determined as described by the previous study [26]: (1) 50 mL NaCl solution (0.01 M) is placed in a 100 mL glass bottle to maintain the ionc strength of the solution, (2) the pH in the solution is adjusted range from 2.0 to 11.0 using 0.1 M of NaOH or HCl solution, (3) 0.1 g MOS is added to the solution, and then (4) the final pH of the solution is measured after 24 h incubation at 25 °C and 100 rpm. The pH_{PZC} is calculated based on the ΔpH (final pH − initial pH) = 0 (Fig. 5). It should be noted that all experiments were performed in duplicate while the control experiment was conducted along with all experiments simultaneously to minimized error.

As shown in Fig. 5, the pH_{PZC} value of moringa oleifera seed (MOS) is 6.7. Thus, the surface charge of MOS is protonated (i.e. positive charge) when the solution pH is lower than their pH_{PZC}, otherwise it was the negative.

Optimization of parameters that influence the removal efficiency

Optimization of initial Pb(II) concentration

Adsorption capacity (mg/g) as a function of initial lead ions concentration is shown in Fig. 6. The adsorption capacity is influenced by its initial concentrations, and the adsorption

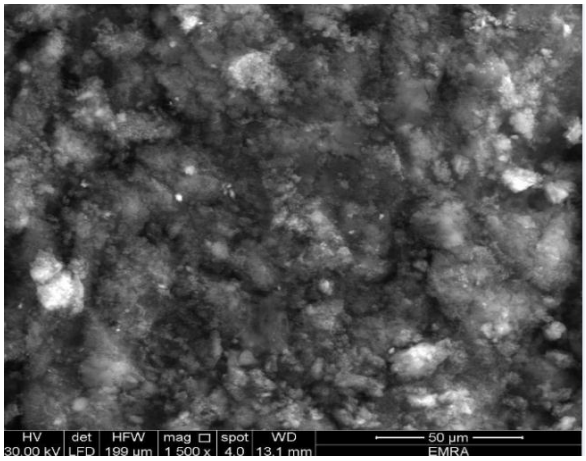

Fig. 3. SEM image of raw MOS

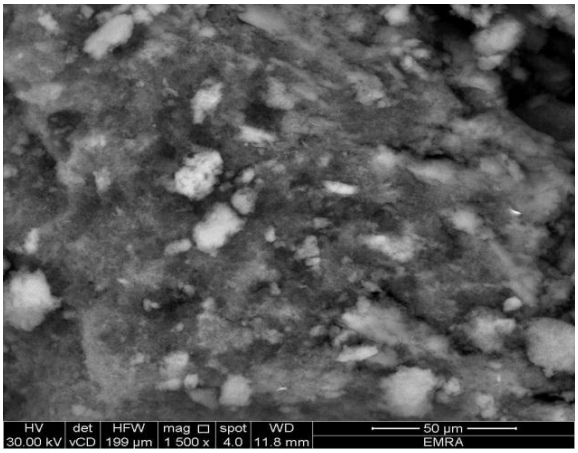

Fig.3. SEM image of MOS loaded-Pb(II)

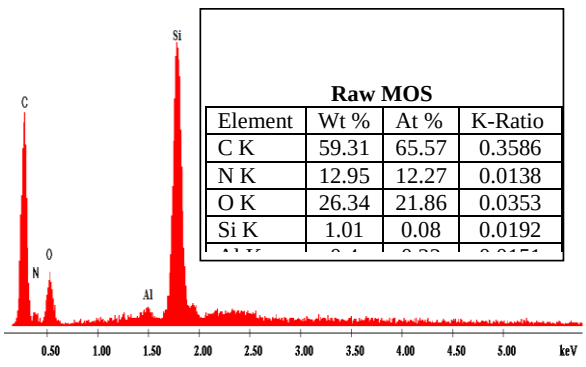

Raw MOS

Element	Wt %	At %	K-Ratio
C K	59.31	65.57	0.3586
N K	12.95	12.27	0.0138
O K	26.34	21.86	0.0353
Si K	1.01	0.08	0.0192

Fig. 4. EDX scanning of raw MOS

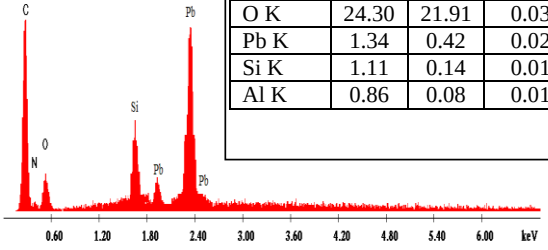

MOS loaded-Pb

Element	Wt %	At %	K-Ratio
C K	59.97	65.57	0.3586
N K	12.42	11.88	0.0138
O K	24.30	21.91	0.0353
Pb K	1.34	0.42	0.0212
Si K	1.11	0.14	0.0122
Al K	0.86	0.08	0.0101

Fig. 4. EDX scanning of MOS loaded-Pb(II)

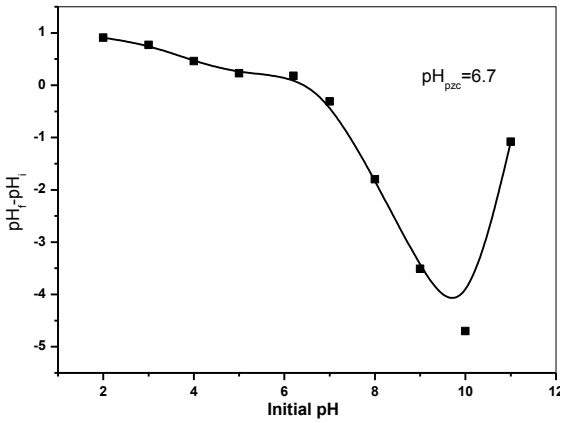

Fig. 5.pH$_{PZC}$ plot of the raw MOS powder

capacity tend to enhance with the increase of initial concentration, counter to removal efficiency. With the increase of initial lead ions concentration from 62 mg/L to 909 mg/L, the adsorption capacity of Pb(II) had a trend of linear increase from 62 mg/l to 909 mg/l. This suggests that the binding sites on MOS surface became sufficient and saturated after the initial lead ion concentrations reached 909 mg/L. It indicates that MOS released a limited amount of binding sites [27]. Fig. 6 shows removal efficiency values as a function of initial Pb(II) ions concentrations. It can be obtained from the figure that MOS is effective in Pb(II) removal from aqueous solutions. The removal percentage of lead ions is influenced by its initial concentrations and the removal efficiency of Pb(II) tend to decline from 83.87-69.30% with the increase of the initial solution concentration. The higher decline rate in Pb(II) removal with increasing initial concentration is pronounced for 909 mg/l. As the concentration further increased, the removal efficiency of Pb(II) decreased dramatically.

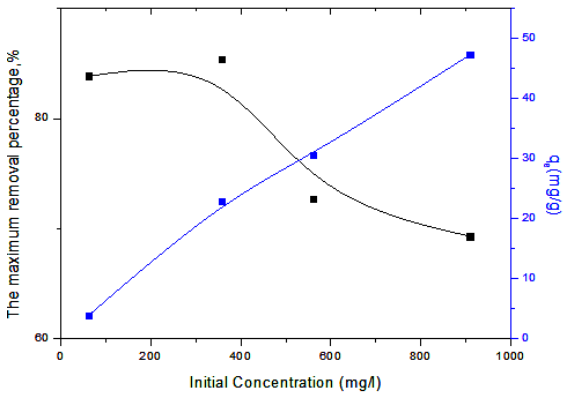

Fig.6. Effect of the initial Pb(II) concentration on the removal percentage

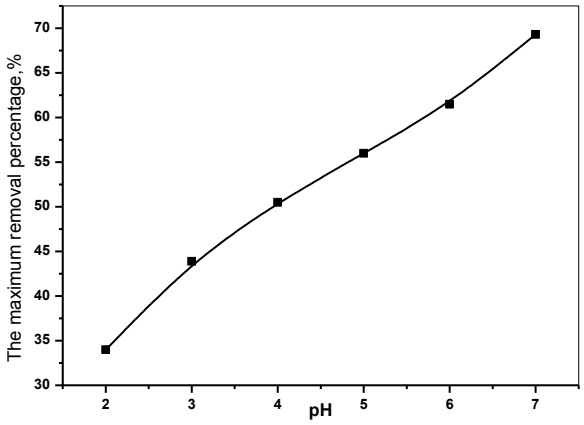

Fig.7. Effect of the solution pH on the removal percentage of Pb(II)

Influence of initial pH

It is well known that the pH of the medium affects the solubility of metal ions and concentration of the counter ions on the functional groups of the biomass cell walls, so pH is an important parameter on bio-sorption of metal ions from aqueous solutions. moringa oleifera seed presents a high content of ionizable surface groups such as carboxyl, ketonic, alcoholic, and amino groups. Presence of these groups is confirmed by FTIR spectroscopic analysis. As shown in Fig. 7 the uptake of free ionic Pb(II) depends on pH, increasing with the increase in pH from 2.0 to 7.0 and then precipitated lead appears in the pH range 7.0–8.0.. At pH values lower than 7.0, Pb(II) removal is partially inhibited, possibly as a result of the competition between hydrogen and Pb(II) ions on the sorption sites, with an apparent preponderance of hydrogen ions, which restricts the approach of metal cations as in consequence of the repulsive force. As the pH lowered, however, the overall surface charge on the biomass cells become positive, which will inhibit the approach of positively charge metal cations. It is likely that protons will then compete with metal ions for ligands and thereby decrease the interaction of metal ions with the cells. The ionization constants of a number of carboxylic acids are above pH 5, so a biomass having carboxylic functional group has positive charge above this pH and negative charge below this pH. The intensity of induced charge on carboxylic group depends upon how lower or higher is the pH. At lower

pH values, carboxyl groups retained their protons reducing the possibility of binding to any positively charged ions. Whereas at higher pHs above 5, the carboxylate ($–COO^-$) ligands attract positively charged metal ions and binding occurs, indicating that the major process is an ion exchange mechanism that involve an electrostatic interaction between the positively charged groups in cell walls and metallic cations. Therefore further experiments are carried out with initial pH value 7 since Pb^{2+} ions hydrolyzes into insoluble $Pb(OH)_2$, which starts precipitating from solutions at higher pH values, making true sorption studies impossible,. One of the most important aspects that have to be evaluated in a bio-sorption study is the selection of suitable part of biomass able to sequester the largest amounts of metal of interest from its solution. One possible preliminary test that may be used to perform this selection is the effect of pH on metal uptake capacity of biomass (Fig. 7). Similar results have been reported in literature for different metal-biomass systems [28].

Effect of agitation time

The adsorption process was fast in the initial phase ~15 min and the adsorption capacities increased quickly to reach 2.55 mg/g. Subsequently the adsorption of Pb(II) sustained at a slower rate until the adsorption rate attained a constant value at its maximum level after approx. 300 min of reaction; maximum levels are found as shown in Fig. 8. The fast initial adsorption rates are attributed to the high number of accessible free functional groups e.g. –OH and $–NH_2$ on the surface of the moringa oleifera seed adsorbent at the start of the adsorption process and less steric hindrance for the approaching lead ions. The slow adsorption process is a result of the reduction in the available adsorption positions and the build-up of lead ions on the surface of the MOS adsorbent; this hinders the diffusion of more lead ions into the MOS pores. Slow diffusion rates are related to pores which are of a similar size to the diffusing adsorbates[29.]MOS is carrying amino groups and thus exhibits much higher uptake capacity. The amino group has an electron pair available for coordination and behaves like a strong Lewis base. The amine nitrogen on MOS has been suggested as the active site for metal ion coordination. A free radical tentatively assigned to one of the MOS hydroxy groups is assumed to be participating in the complex formation [30].

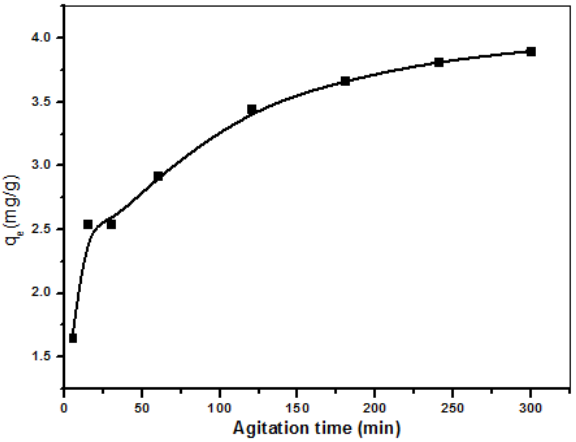

Fig.8. Effect of the agitation time on the Pb(II) uptake

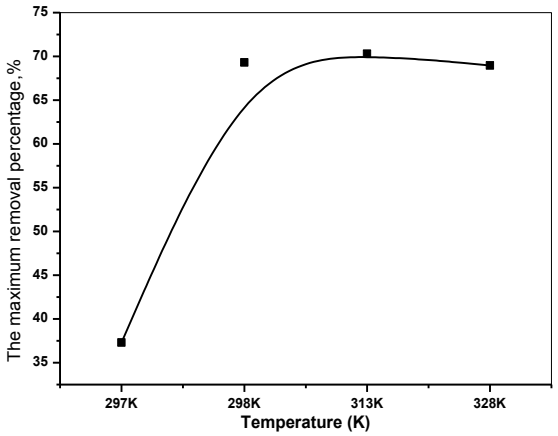

Fig.9. Effect of the solution temperature on the removal percentage of Pb(II)

Effect of temperature

To study the effect of this parameter on the kinetics of lead sorption by MOS, we selected the following temperatures: 277, 298, 313 and 328˚K. The results obtained and presented in Fig. 9 indicate that an increase of the temperature in the interval 277 to 313K deals with an increase in the capacity of lead ions sorption at equilibrium: 25.45 mg/g at 277˚K and a high capacity of sorption about 47.97 mg/g between 298˚K and 313K. Beyond 328˚K, we notice a reduction in the capacity of lead ions sorption at equilibrium: 47.07 mg/g. The reduction of the removal in the interval of

temperature 313 to 328˚K means that the process of Pb(II) sorption by MOS is exothermic. Similar results have been reported for the sorption of lindane by chitin in seawater at three temperatures 5°C, 22°C and 45°C [31]. The time necessary to reach equilibrium of sorption for the different studied temperatures is practically the same about 3 hrs, except the temperature of 277˚K of which the time of equilibrium is about 5 hrs. According to the literature, results of study of the effect of the temperature on the phenomenon of sorption for different metal–biomaterials systems are disparate. If sorption is governed only by physical phenomena, an increase in temperature will be followed by a decrease in sorption capacity. Temperature could influence the desorption step and consequently the reversibility of the sorption equilibrium.

Effect of the MOS dose

In order to maximize the interaction between active sites of adsorbent and metal ions, the effect of adsorbent dose(0.333 - 0.666 - 1.332 - 1.998 - 2.664 - 3.333 g) on the adsorption capacity and removal efficiency has been studied under the initial condition of 50 mL of 909 mg/L metal ions at 298 ˚K and pH ~7. Under experimental conditions; the effect of adsorbent dosage on adsorption of lead ions onto MOS is carried out and the results are presented in Fig. 10. As can be seen from this figure, adsorption capacity is found to decrease proportionally with an increase in the amount of MOS. In contrast, the Pb(II) removal efficiency of MOS increased with increased adsorbent amount, which can be due to the large number of vacant adsorption sites and the greater surface area hence favoring more Pb(II) adsorption. The decrease in adsorption capacity is attributable to the splitting effect of the concentration gradient between sorbate and sorbent with increased MOS concentration causing a decrease in amount of Pb(II) adsorbed onto unit weight of MOS. This phenomenon was also found by **Anupam et al.**[32] using a powdered activated carbon, for the removal of hexavalent chromium from aqueous solution. As the initial Pb(II) concentration is fixed, Pb(II) ions can occupy only a certain amount of active sites. Thus, an additional raise in the number of active sites of MOS does not influence the total Pb(II) ions adsorbed. It can be concluded that for each ion concentration there is a corresponding adsorbent dose at which adsorption equilibrium will be established [33].

Effect of shaking speed

The distribution of the adsorbate ions in the aqueous solution is generally affected by agitation speed. The effect of the shaking speeds (100, 200, 300, 400, 500 and 600 rpm) on the adsorption of Pb(II) onto MOS is performed and the results are shown in Fig. 11. The rate of shaking has a clear effect on the amount of Pb(II) uptake which may indicate that mass transfer is a key factor in controlling the rate. The maximum removal percentage of Pb(II) adsorbed increased from 69.3 to 76.23% when the rate of shaking increased from 100 rpm to 400 rpm. This can be attributed to the increase of the mobility of the system and decrease in the film resistance to mass transfer surrounding the adsorbent particle [34]. As demonstrated, this occurs because, the stirring rates from 100 to 400 are in the average range of agitations rates, and usually in this range a slight change in adsorption behavior take place. Nevertheless, there is a significant decrease observed with regards to the MOS efficiency in experiments where the mixing speed was above 400 rpm. This decrease is determined to be 67.32% at 600 rpm which is assumed to be a result of the lead ions not being sufficiently MOS inside during the generation of the particles due to the vortex effect at high mixing speeds.

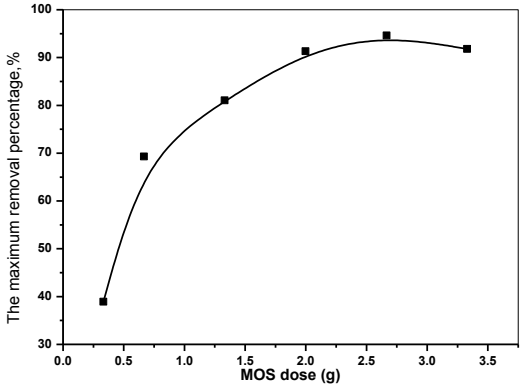

Fig.10. Effect of the MOS dosage on the removal percentage of Pb(II)

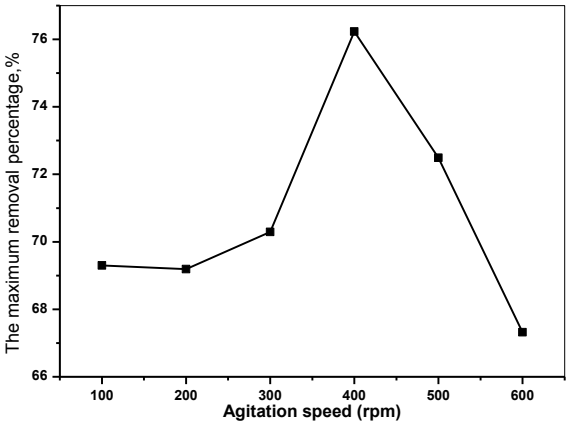

Fig.11. Effect of the agitation speed on the removal percentage of Pb(II

Distribution coefficient (K_D)

The solid–liquid distribution coefficient (K_D) of lead ions on MOS and in solution after adsorption can be calculated by Eq. (3):

$$K_D=q_e/C_e \text{----------} \quad (3)$$

where, Ce (mg/L) is the liquid-phase concentrations of Pd(II) at time zero, K_D is The distribution coefficient and q_e (mg/g) is The adsorption capacity at equilibrium. The distribution coefficient K_D increases from 0.04465 to 0.177674 L mL^{-1} with an increase in the solution temperature from 277˚K to 323˚K, while declines from 0.177674 to 0.177674 L mL^{-1} with increasing the solution temperature from 313˚K to 323˚K (observed from Fig. 12). The change law of K_D may be caused by the fact that the adsorptive sites are used effectively for the solution temperature from 277˚K to 313˚K, whereas are not for the solution temperature of 323˚K. The similar research results were reported by **Ding et al., 2012**[35].

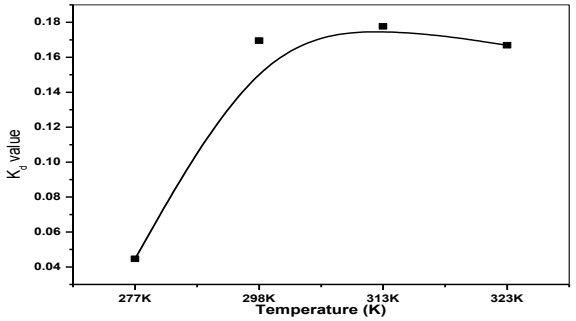

Fig.12. The distribution coefficient of Pb(II)

Adsorption isotherms

Adsorption isotherms describe equilibrium and the interaction between adsorbate and adsorbent. Equilibrium is established when the adsorbate concentration in the solution is in dynamic balance with adsorbent concentration. The isotherm adsorption constants quantify the affinity of the MOS adsorbent surface properties towards lead(II) ions. Experimental data obtained are fitted to widely used isotherm models: Langmuir [36], Freundlich [37], Temkin.[38] and Dubinin-Radushkevich[39]

Langmuir isotherm

Langmuir models suggest that adsorption took place with a mono-molecular/ions layer arrangement on adsorbent surfaces and there is no interaction between the adsorbed molecules or ions. The simple linearized form of Langmuir isotherm equations:

$$\frac{C_e}{q_e}=\frac{1}{K_L Q_{max}}+\frac{C_e}{Q_{max}} \quad \text{-------} \quad (4)$$

Where C_e is the equilibrium concentration of adsorbate (mg/l), q_e is the amount of soluted sorbate at equilibrium (mg/g), K_L is the Langmuir adsorption constant (L/mg) and Q_{max} (mg/g) is the theoretical maximum adsorption capacity (mg/g).

The values of Q_m and K_L constants and regression coefficients for Langmuir isotherm $\frac{C_e}{q_e}$ are evaluated from a plot of q_e versus C_e(Fig.13). The maximum mono-layer capacity Q_m is 70.52 mg/g at T = 298K. The Langmuir constants are given in Table 1. Regression coefficients R^2 for different concentrations studied show that the Langmuir isotherm poor fitted with the experimental data. Regression coefficient obtained for temperature 298 K is (R^2 = 0.85206). This may explain that adsorption is an endothermic process and higher temperature leads to bio-molecules decomposition.

Separation factor (R_L)

The shape of the Langmuir isotherm can be used to predict whether a sorption system is favorable or unfavorable in a batch adsorption process. Accordingly, the essential features of

the Langmuir isotherm was expressed in terms of a dimensionless constant called the equilibrium parameter, R_L, which is defined by the following relationship (Eq. (4)):

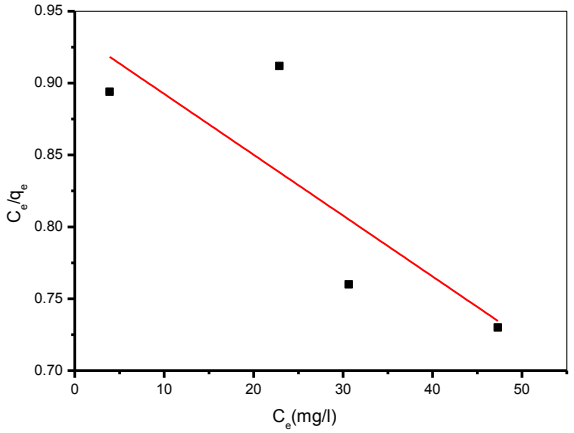

Fig.13. The Langmuir plot of Pb(II) adsorption

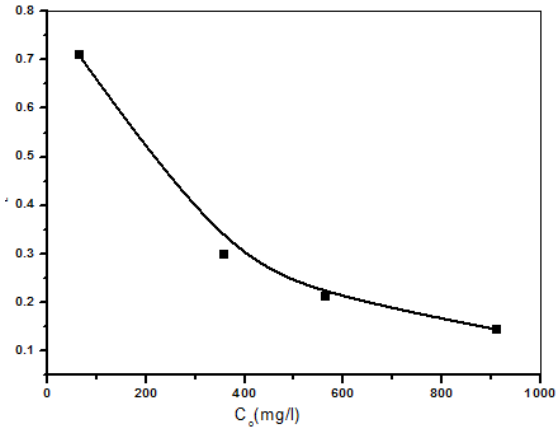

Fig. 14. Separation factor profile for bio-sorption of Pb(II) as function of initial lead concentration by MOS

$$R_L = \frac{1}{1 + K_L C_0} \quad \text{-------} \qquad (5)$$

where R_L is the a dimensionless equilibrium parameter or separation factor, K_L the constant from Langmuir equation and C_o the initial metal ion concentration. The parameter, R_L, indicates the shape of the isotherm and nature of the sorption process. R_L value between 0 and 1 represents favorable isotherm. The values of R_L for Pb(II) for MOS biomass was calculated from Eq. (4) and plotted against initial metal ion concentration. The data showed that, the sorption of Pb(II) on MOS biomass decreased as the initial metal ion concentration increased from 62 to 909 mg/L, indicating that adsorption is even favorable for the higher initial metal ion concentrations (Fig. 14) [40]. The sorption process was favorable for Pb(II) removal at all concentrations investigated. According to this classification, removal ability tends to be in the order: 909 mg/l > 561 mg/l > 357 mg/l > 62 mg/l. The trend presented by R_L in Fig. 14 is also providing information that the MOS biomass is more effective and excellent adsorbent for Pb(II) at lower metal concentrations (up to 357 mg/L).

Surface coverage values (θ)

To account for the adsorption behavior of the Pb(II) on the *MOS* biomass, the Langmuir type equation related to surface coverage is used. The equation is expressed as follows (Eq. (6)).

$$\Theta = K_L C_o(1- \theta) \text{----------} \qquad (6)$$

where K_L is the adsorption coefficient, C_o the initial concentration and θ the surface coverage.

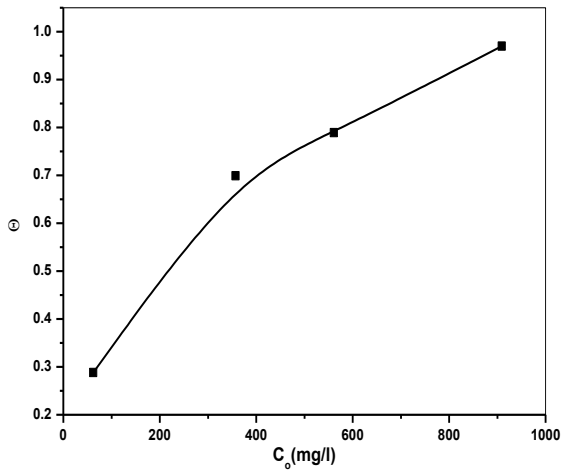

Fig. 15. A plot of surface coverage (θ) against concentration of Pb(II) (mg/L) for MOS biomass

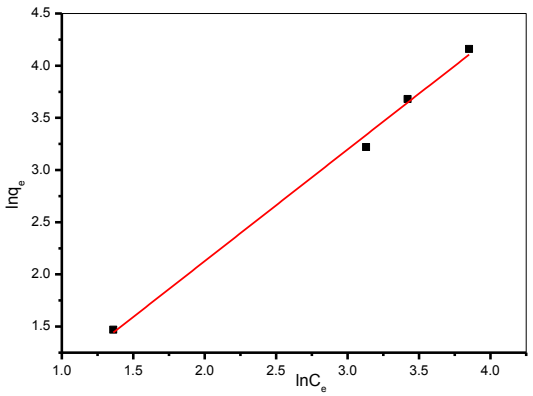

Fig.16. The Freundlich plot of Pb(II) adsorption

The fraction of biomass surface covered by metal ion is studied by plotting the surface coverage values (θ) against Pb(II) concentration. The data is presented in Fig. 15. The figure shows that, increase in initial metal ion concentration for MOS biomass increases the surface coverage on the biomass until the surface is nearly fully covered with a monomolecular layer [40]. Further examination of Fig. 15 reveals that the surface coverage ceases to vary significantly with concentration of Pb(II) at higher levels and the reaction rate becomes independent of the Pb(II) concentration. Surface coverage value indicated that MOS was more effective in uptake of Pb(II) from aqueous solutions at all initial concentrations.

Freundlich isotherm

Freundlich isotherm model suggests that molecules are adsorbed as a mono molecular layer or multilayer on heterogeneous adsorbent surfaces and there is an interaction between the adsorbed molecules or ions. The simple form of Freundlich model is described by:

$$\ln q_e = \ln q_e = \ln K_F + \frac{1}{2}\ln C_e \qquad (7)$$

where K_F(mg/g) and n are isotherm constants indicate the capacity and intensity of the adsorption, respectively.

The Freundlich constant K_f gives information about bond energies between the adsorbent and the metal ions. A plot of Lnq_e versus LnC_e is a straight line defined by a slope and intercept LnK_f (Fig.16), plot (B). The adsorption mechanism fits well for the Freundlich model. Freundlich parameters are given in Table 1. Regression coefficient obtained for temperature 298 K is $R^2 = 0.9220$ fitted quite well with the experimental data. As seen from Table 1, the adsorption of Pb(II) on MOS adsorbent is favorable.

Temkin isotherm

Temkin isotherm suggests an indirect interaction between adsorbate and adsorbent. The heats of adsorption of molecules decrease for the first layers and then increases with coverage increase. Furthermore, the isotherm model contains a factor related to adsorbent-adsorbate interactions noted A_T. The Temkin model (Fig. 17)is described by the following equation:

$$q_e = \left(\frac{RT}{b_T}\right)\ln A_T + \left(\frac{RT}{b_T}\right) ln C_e \text{ ---} \qquad (8)$$

Where C_e is the equilibrium Pb(II) concentration in solution (mg/L), q_e is the equilibrium Pb(II) concentration on the adsorbent (mg/g), $B_T = \left(\frac{RT}{b_T}\right)$, B_T is the Temkin constant (KJ/mol) related to adsorption heat, T is the absolute temperature (K), R is the gas constant (8.314 J/mol K), and A_T is a Temkin binding constant (L/g). B_T is a constant related to heat of adsorption (J/mol) (B_T) and (A_T) can be calculated from the slope and intercept of the plot of q_e vs. $ln C_e$. Experimental results are fitted to The regression value R^2 obtained for Temperature 298 K is 0.92876, the others estimated Temkin parameters are presented in Table 1.It also has high R^2 (0.92876) for Temkin isotherm equation (Table 1). With no consideration of extremely high or low initial concentrations, the model describes that the adsorption heat of metal ions in the layer decreases linearly with coverage [41]. The lowA_T value indicate a low potential between adsorbent and adsorbate and may facilitate the interaction between adsorbent and adsorbate.

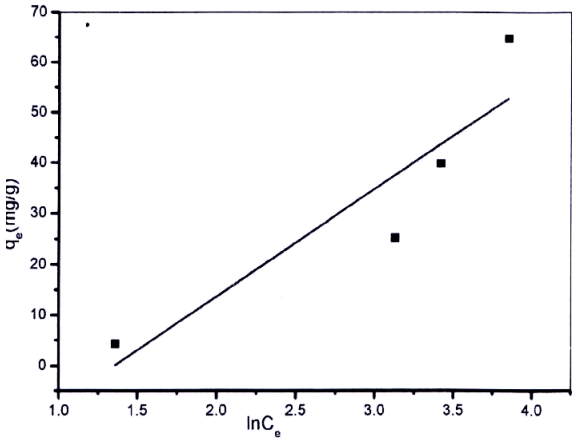

Fig.17. The Temkin plot of Pb(II) adsorption

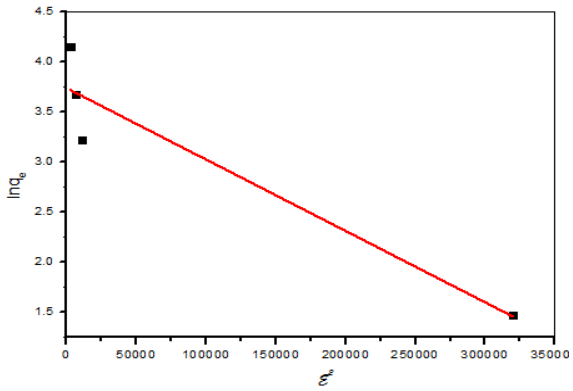

Fig.18. The D-R plot of Pb(II) adsorption

Dubinin-Radushkevich (D-R) isotherm

Dubinin-Radushkevich isotherm expresses the adsorption mechanism on a heterogeneous and porous surface with variable parameters. The model is described by the following equation:

$$\ln q_e = \ln(X_{D-R}) - \beta\varepsilon^2 \text{-----} \quad (9)$$

Where X_{D-R} is the theoretical monolayer saturation capacity (mg/g), β is the Dubinin–Radushkevich model constant (mol^2 J^{-2}). ε is the polanyi potential and is equal to ε is the D-R isotherm constant and can be expressed as follows:

$$\varepsilon = RT\ln\left(1+\frac{1}{C_e}\right) \text{-----} \quad (10)$$

C_e is the equilibrium Lead(II) concentration (mg/L), q_e is the equilibrium Lead(II) concentration on the adsorbent (mg/g), X_{D-R} is theoretical isotherm adsorption capacity (mg/g), β is D-R isotherm constant (mol^2/kJ^2). R is the gas constant (8.314 J.mol^{-1}.K^{-1}),T is temperature (K). The free energy per molecule or ion of adsorbate designed E can be calculated as follows.

$$E_{D-R} = \frac{1}{\sqrt{-2\beta}} \text{-------} \quad (11)$$

From the magnitude of E, the kind of bio-sorption mechanism can be defined as follows: The magnitude of E between 8 and 16 kJ/mol corresponds to a chemical ion exchange process. The magnitude of E < 8 kJ/mol corresponds to a physical bio-sorption process. The obtained value of E in this work was 0.112175 kJ/mol for studied concentrations which is higher than the adsorption energy values previously enumerated. This indicates that adsorbate-adsorbent interaction is governed by a physical adsorption process. This result (Fig. 18 and Table 1)will be confirmed by the thermodynamic study. However, in the case of the sorption of Pb(II) on bio-chars, a low R^2 was found with the Dubinin–Radushkevich model and this indicated that the application of this model in this research is limited [42].

A comparison between isotherms models: Langmuir, Freundlich, Temkin and Dubinin-Radushkevich for different concentrations (62, 357, 516 and 909 mg/l). By comparing the regression coefficient R^2 illustrated in Table 1, the Lead (II) adsorption on MOS biosorbent in this study is more fitted to Temkin, Freundlich more than Dubinin-Radushkevich and Langmuir model, the least fitted one to experimental data. Yet, Lead ions are, probably, adsorbed as a multi molecular layer on a heterogeneous adsorbent surfaces. Furthermore, adsorption process is predominantly physical. As though, Langmuir

Table 1.Langmuir, Freundlich, Temkin and Dubunin Radushkevich isotherm Model constants for adsorption of Lead (II) on MOS adsorbent.

Freundlich			Langmuir				
1/n	K_f (mg/g)	R^2	Q_{max} (mg/g)	K_L (L/mg)	C_o(mg/l)	R_L	R^2
0.73988	0.823	0.9220	70.52	0.0066	62	0.7123	0.85206
					357	0.30070	
					561	0.2148	
					909	0.14448	
D-R				Temkin			
β(mol^2/kJ^2)	X_{D-R} (mg/g)	E_{D-R} (kJ/mol)	R^2	A_T (L/min)	B_T		R^2
3.97x10^{-5}	33.2621	0.112175	0.9171	0.1308	12.0008		0.92876

model diverges with the experimental data for higher metal concentration or for extended contact time between adsorbent and metal solution.

Adsorption kinetics

The kinetic experimental data obtained was fitted to the linearized form of the pseudo-first, pseudo-second and Elovich models [43, 44 and 45, respectively].

The pseudo-first order model

The pseudo-first order model equation is for the adsorption in a liquid-solid system. It considers that the adsorbate uptake is directly proportional to the difference of the concentration saturation level.

The linearized form of pseudo-first order model equation is:

$$ln(q_e - q_t) = ln\, q_{e,1,cal} - k_1 t \quad \text{---} \quad (12)$$

q_e is the equilibrium concentration of Lead ions on the adsorbent and q_t is the Pb(II) concentration at time t (mg/g). k_1 is the first-order model constant (min^{-1}).The plot of $Ln(q_e - q_t)$ versus t is used to calculate k_1 and q_e from, respectively, the slope plot and the intercept plot (Fig.19).

It was found that k_1 of the pseudo-first order rate constant shows an increase with an increase in the initial Pb(II) concentration at 62 mg/l, 357 mg/l and 909 mg/l and then decrease in the Pb(II) concentration (561 mg/l) values (Table 2). This is attributed to competition between higher levels of Pb(II) ions for the adsorbent active sites. The tendency that a k_1 declines with increasing C_o suggests that it is quicker for a system with a lower C_o to attain a definite fractional uptake.

The pseudo-second order model

The pseudo-second order model is based on chemisorption. The adsorbate interacts with the adsorbent surface by establishing a covalent chemical bond. The pseudo-second order model equation is expressed as follows: The linearized form of pseudo-second order model is given by;

$$\frac{t}{q} = \frac{1}{k_2 q_{e,2}^2} + \frac{1}{q_{e,2}} t \quad \text{------} \quad (13)$$

The model parameters obtained at different initial Pb(II) concentrations after fitting the pseudo-first and pseudo-second order kinetic models are given in Fig. 20 and Table 2. For MOS adsorbent, the high correlation coefficients indicated that the pseudo-second order ($R^2 > 0.99$) models described the Pb(II) adsorption kinetic well compared to the pseudo-first order ($R^2 < 0.98$). Moreover, the pseudo second order model q_e predicted values were in better agreement with the experimental values. As the pseudo-second order model dealt with processes that involves intra-particle and external liquid film diffusion as well as surface adsorption, imply that the pseudo second order model explains more accurately the adsorption mechanism of Pb(II) onto MOS. Inferably, based on the kinetic parameters, the pseudo-second order model data suggests that the rate limiting step during Pb(II) onto MOS was chemisorption. Thus, chemisorption, which involves electrostatic attraction and chemical bonding between the adsorbate and adsorbent [46], was responsible for the adsorption of Pb(II) on the MOS On the other hand, the second-order rate constant (k_2) shows a gradual increases with an increase in the initial Pb(II) concentration.

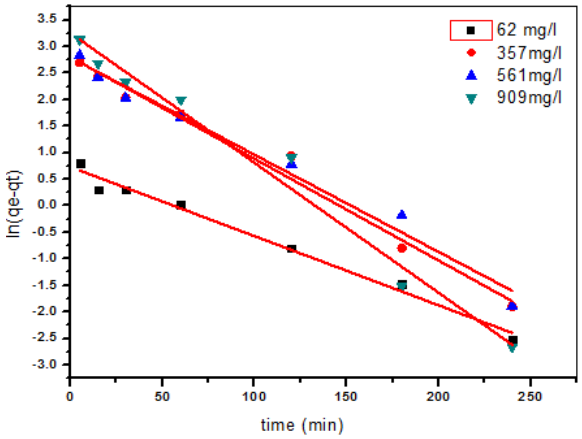

Fig.19. Pseudo-first order plot of Pb(II) adsorption.

Elovich model

Elovich model is useful in chemical adsorption processes and is suitable for highly

heterogeneous systems The Elovich equation is defined as follows:

$$q_t = \frac{1}{\beta}\ln(\alpha\beta) + \frac{1}{\beta}\ln t \quad \text{----} \quad (14)$$

where q_t is the amount of Pb(II) adsorbed on MOS at a time t, α is the initial Pb(II) adsorption rate (mg/g min^{-1}) and β is the desorption constant related to the surface coverage and the activation energy for chemisorption (g/mg). The slope plot of qt versus $Ln(t)$ is used to calculate Elovich coefficients α and the intercept of the plot is used to calculate β (Fig. 21).

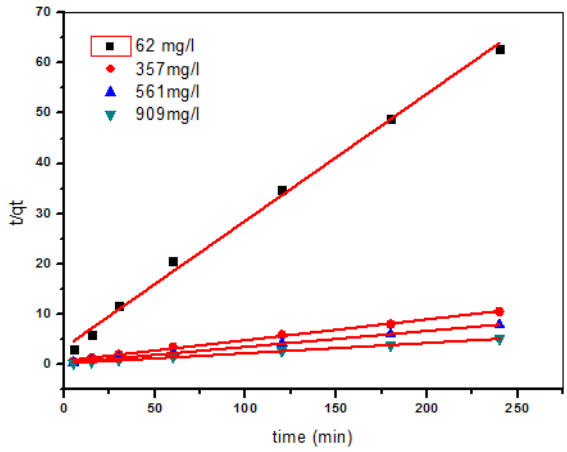

Fig.20. Pseudo-second order plot of Pb(II) adsorption

The Elovich and intra-particle kinetic models parameters for adsorption of Pb(II) on the MOS at different initial Pb(II) concentrations are given in Table 3. The Elovich model fitted the results of MOS adsorbent better at 62 mg/l, 357 mg/l and 561 mg/l (R^2 = 0.99256, 0.98962 and 0.98779, respectively) but didn't fit well when the concentration was 909 mg/l (R^2 = 0.96586).

The intra-particle diffusion model

The intra-particle diffusion model*:* this model is normally used for a deeper understanding of the adsorption mechanism. A plot of q_t *versus* $t^{0.5}$ (Fig.22) should be a straight line when the adsorption process is controlled by the intra-particle diffusion where the adsorbate ions diffuse in the intra-particle pore of the adsorbent. However, more than one step could govern the process if the data exhibit multi-linear plots. The intra-particle diffusion co-efficient, k_{id}, can be determined by fitting the experimental data in the intra-particle diffusion model [47].Intra-particle diffusion model based on the theory proposed by Weber and Morris was used to identify the diffusion mechanism as well:

$$qt = k_{int}t + C^{1/2} \quad \text{----------} \quad (15)$$

where k_{int} is the intra-particular diffusion rate constant (mg/g $min^{-1/2}$).

The dual nature of the curve (Fig.22) was obtained due to the varying extent of sorption in the initial and final stages of adsorption experiment. This can be attributed to the fact that in the initial stages the sorption was due to the boundary layer diffusion effect, whereas in the later stages (linear portion of the curve) it was due to the intra-particle diffusion effects. The intercept of the plot reflects the boundary layer effect. The larger is the intercept and greater will be the contribution of the surface sorption in the rate controlling step. If the regression in the plot of q_t versus $t^{(1/2)}$ is linear and passes through the origin, then intra-particle diffusion is the sole rate-limiting step. However, the linear plots at each concentration did not pass through the origin. This deviation from the origin may perhaps be due to the difference in the rate of mass transfer in the initial and final stages of adsorption. This indicated that there is some degree of boundary layer control and this further showed that the intra-particle diffusion was not only the rate-limiting step, but also be the rate controlling of sorption or all may be operating simultaneously. Our experimental data (Table 3), revealed that the constant values the intra-particle diffusion model. However, it was observed that, there are multi- linear portions that explain the adsorption stages; these are the external mass transfer at initial period, intra-particle diffusion of Pb(II) on the adsorbent.

Sorption thermodynamics

With the purpose of investigating the spontaneity and the thermodynamic properties of the adsorption process, the thermodynamic studies were carried out and three important parameters namely the Gibbs free energy

change (ΔG°), standard enthalpy change (ΔH°) and standard entropy change (ΔS°) were obtained by Van't Hoff equation (Eq. 15) and Gibbs-Helmholtz equation (Eq. 16) [46]:

$$\ln[K_d] = ((S^\circ)/R - ((H^\circ)/RT \quad \text{-- (16)}$$

$$\Delta G^o = -RT\ln K_d \text{----------} \quad (17)$$

where R is universal gas constant (8.314 J/mol·K), T is the temperature (K)

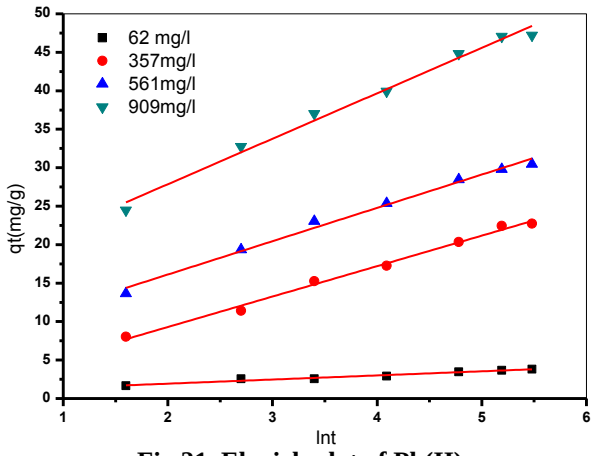

Fig.21. Elovich plot of Pb(II)

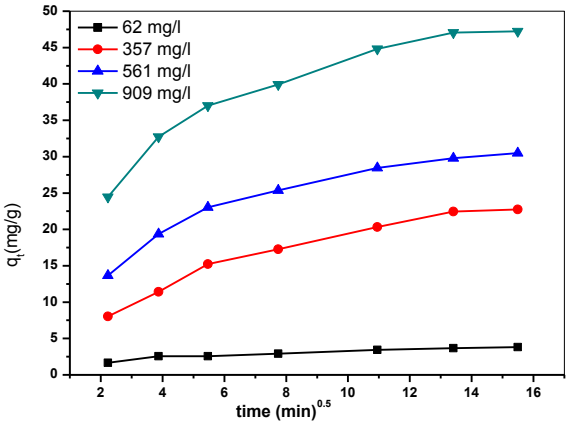

Fig.22. Intra-particle diffusion plot of Pb(II)

The values of ΔH° and ΔS° can be acquired from the slopes and intercepts of the plots of $\ln K_d$ versus 1/T, which were plotted in Fig. 23. The thermodynamic parameters were summarized in Table 4.

Fig. 23 exhibits an increasing tendency of ion uptake as temperature rises from 277 K to 323 K. As listed in Table 4, the positive values of ΔH° enunciate all investigated adsorption processes are endothermic and that higher temperature is beneficial to the adsorption processes, which is in agreement with the conclusion of the isothermal discussion. Positive values of ΔS° imply an increase in randomness. The reason behind it might be the release of free water molecules during the adsorption process. According to coordination theory, the metal ions (Pb^{2+}) provide empty orbits, while oxygen atoms in water molecules provide lone pairs of electrons, to form hydration ions in the absence of adsorbents in solution. After adsorption, metal ions are chelated by active groups on the MOS materials, and water molecules previously bonded with metal ions are released to bulk solution as free molecules, leading to an increase in the total amount of ions in the existing system. As a result, the ΔS° values gradually increase. Besides, the values of ΔS° and ΔH° obtained from Pb-MOS systems are markedly large, also implying Pb-MOS has high affinity for the lead ions. The positive values of ΔG° for all experimented temperature (Table 4) verify the adsorption processes of lead ions onto adsorbents are thermodynamically non feasible and non spontaneous.

In order to further support the assertion that the adsorption is the predominant mechanism, the values of the activation energy (E_a) and sticking probability (S*) were estimated from the experimental data. They were calculated using a modified Arrhenius type equation related to surface coverage [48]. The sticking probability, S*, is a function of the adsorbate/adsorbent system under consideration and is dependent on the temperature of the system. The parameter S* indicates the measure of the potential of an adsorbate to remain on the adsorbent indefinitely. It can be expressed as in Table4. The effect of temperature on the sticking probability was evaluated throughout the temperature range from 277 to 328 K by calculating the surface coverage at the various temperatures. Table 4 also indicated that the values of $S^* \leq 1$ (0.38676) for the MOS, hence the sticking probability of the Pb (II) ion onto the adsorbent system are very high.

Table 2. Parameters of pseudo first, pseudo second order kinetic models.

C_0 (mg/l)	Pseudo-first order				Pseudo-second order			
	h	$q_{e,1,cal}$	k_1	R^2	$q_{e,2,cal}$	k_2	h	R^2
62	0.0269	2.08	0.01302	0.98223	3.959	0.01885	0.295502	0.99654
357	0.3132	16.44	0.01916	0.97868	24.201	0.002399	1.4055	0.99891
561	0.1152	16.30	0.01831	0.97559	31.525	0.003033	3.014499	0.99886
909	0.6328	25.86	0.02447	0.98259	40.160	0.003504	5.6516	0.99557

Table 3.Parameters of Elovich and intra particle diffusion kinetic models.

C_o (mg/l)	Elovich model			Intra-particle diffusion		
	α	β	R^2	K_{int}	C	R^2
62	0.97668	1.86511	0.99256	0.14771	1.69591	0.92217
357	1.725	0.252753	0.98962	1.08522	7.60832	0.86274
561	3.188	0.23094	0.98779	1.15723	14.52828	0.86745
909	4.4899	0.16920	0.96586	1.58424	25.64523	0.90671

Table 4- Thermodynamic parameters

Temp.	ΔG^0 KJ/Mol	ΔH^0 KJ/Mol	ΔS^0 J/mol K	R^2	S*	Ea KJ/Mol	R^2
277	7.1597283						
298	4.397442	19.4928	46.8143	0.58244	0.38676	3.202813	0.58234
313	4.49622						
328	4.88205						

$$S^* = (1-\theta)\, exp\left(\frac{E_a}{RT}\right) \text{------} \quad (18)$$

The sticking probability, *S**, is a function of the adsorbate/adsorbent system under consideration and is dependent on the temperature of the system.

$$\theta = 1 - \frac{C_e}{C_0} \text{---------} \quad (19)$$

where C_0 and C_e are the initial and equilibrium metal ion concentrations, respectively

The combination of Eqs. (18) and (19) gives the equation (20):

$$ln\frac{C_e}{C_0} = ln\, S^* + \frac{E_a}{RT} \text{----------} \quad (20)$$

The values of E_a and S^* were obtained from the slope $\left(\frac{E_a}{R}\right)$ and intercept $ln S^*$, respectively, of the plot of $\ln\frac{C_e}{C_o} vs. \frac{1}{T}$. (Fig. 24)>

Sorption activation energy

According to Arrhenius equation, activation energy of the adsorption (E_a,KJ/Mol) can be calculated using the above equation. The magnitude of activation energy gives an idea about the type of adsorption which is mainly physical or chemical. Low activation energies (<40 kJ mol^{-1}) are characteristics for physical adsorption, while higher activation energies (>40 kJ mol^{-1}) suggest chemical adsorption [49]. According to activation energy obtained for the adsorption of lead ions onto the MOS was 3.202813 kJ/mol indicates that the

adsorption process is physisorption. The low value of E_a suggests that the energetic barrier against the adsorption of metal ion is easy to overcome; therefore, adsorption process occurs rapidly [50].

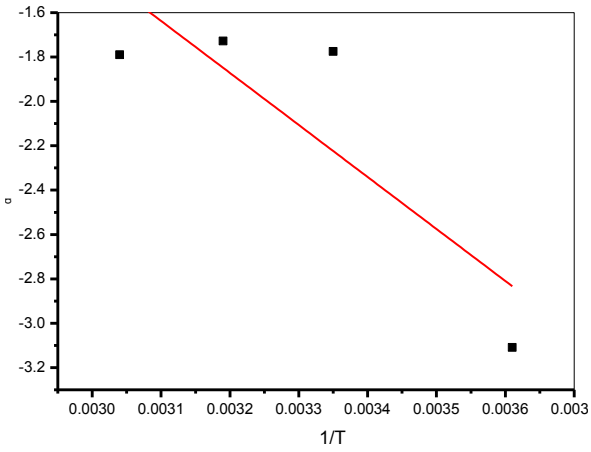

Fig.23. Van,t Hoff plot of Pb(II) adsorption

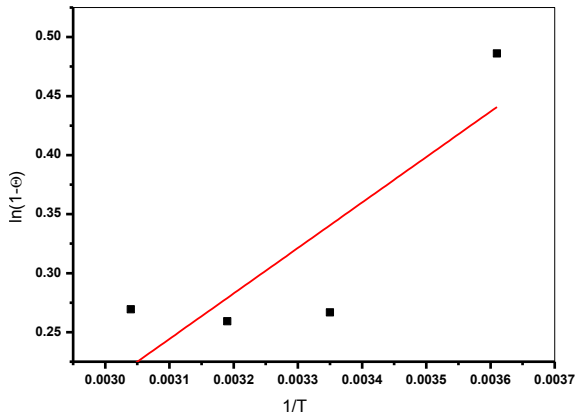

Fig.24. Sticking probability plot of Pb(II) adsorption.

Adsorption behavior of both Pb(II) and Cd(II) in binary system

The adsorption capacities of moringa oleifera seed for both Pb(II) and Cd(II) were investigated at pH ~7 in the temperature range of 4–55°C, and the results are shown in Fig. 25. It can be seen that the adsorption capacities of these ions on the adsorbent increased till the metal ions uptake values reached the stage of equilibrium at 35 °C.. This was attributed to the increased collision efficiency between the adsorbent and these ions in solutions with the temperature increasing. Meanwhile, higher the environment temperature is, hardly the de protonation reaction of functional groups is, which could make more carboxyl and amino groups available for heavy metal ions removal. However, beyond 40 °C for both ions, the adsorption capacities were lowered, possibly due to the exothermic nature (physical or chemical bonds between MOS adsorbent and both Pb(II) and Cd(II) in the adsorption process. With increasing of the solution temperature (>40 °C), the adsorption capacities of Cd(II) no longer enhanced and almost remained the constants. This was limited the further improvement of adsorption capacity. However, the Pb(II) uptake was increased with the temperature increasing (>40 °C). A similar result was obtained by Wei et al., 2016 [51]. The results of the competitive adsorption of Cd(II)-Pb(II) have demonstrated that the Cd(II) ions presented a higher affinity for the cationic sites of the MOS than for Pb(II) ions. For a metal concentration at equilibrium of 100 mg/l, the selectivity was calculated as the maximum removal percentage (Fig.25). The affinity in the adsorption capacities of the MOS towards the metals may be ascribed to ionic radius of the metal cations, Pb (1.19 Å) < Cd (0.97 Å).

Adsorption Mechanism

According to the discussion above, it can be roughly inferred that the possible mechanisms of removing metal ions on moringa oleifera comprise physical and chemical adsorption. On the one hand, the electrostatic attraction and ionic diffusion play an important role in the adsorption process. On the other hand, the N and O atoms are expected to exhibit a strong affinity for cadmium and lead ions [52]. The nitrogen-bearing and oxygen-bearing functional groups can provide numerous active adsorption sites to form strong chelation with cadmium and lead ions in the aqueous solution. The adsorption process might be briefly described as following: the metal ions in the aqueous solution are attracted to the MOS surface by the electrostatic force at first. Then, the ions diffuse into the pore entrance

and pore interior followed by contacting with functional groups. Finally, the ions are fixed with the nitrogen- and oxygen-containing groups by chelation and/or ion exchange, forming a stable binding structure.

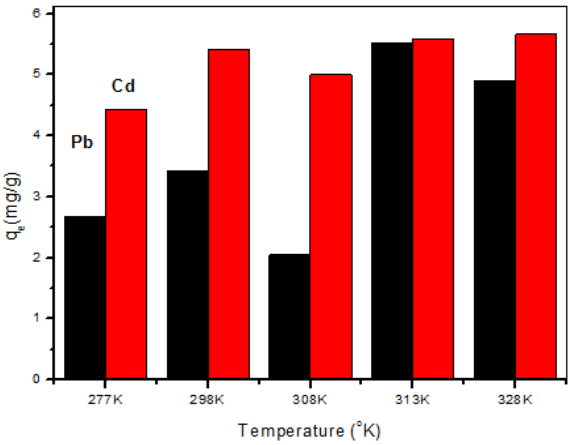

Fig.25. Effect of solution temperature on the removal percentage of Pb (II) and Cd (II) uptake in binary system

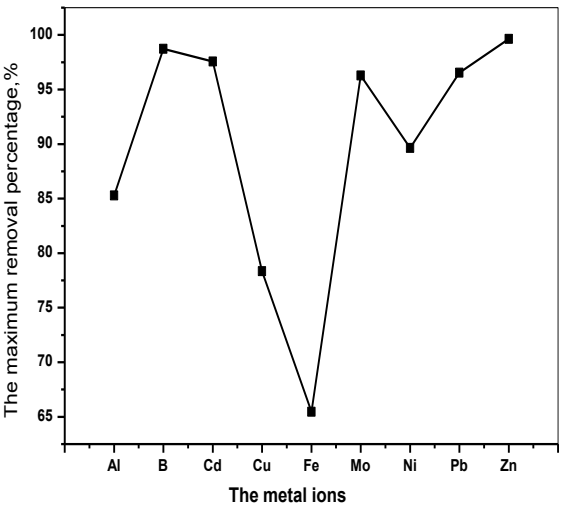

Fig .26. The maximum removal percentage of different ions presented in rare wastewater.

Contaminated real wastewater

The raw effluent sample was collected from the Agriculture Research Center, Giza city, Giza Governorate, South of Cairo Governorate, Egypt. This Agriculture Research Center discharges its effluents into the sewer system of the Giza city and sometimes directly into the ground water (Fig. 26). The sample was collected in three plastic containers, filtered through the Whatman No. 90 filter paper and mixed together, stored, and refrigerated at 4 °C. The effluent sample was analyzed by standard methods (ICP) to evaluate the pollution load of raw wastewater. The different physicochemical parameters such as temperature, pH, conductivity and total dissolved solids (TDS) were analyzed. The average values of such parameters water are presented in Table 5.

Table 5 shows the characteristic results of the real wastewater. Fig. 26 shows the results of the batch adsorption technique using powder from Moringa oleifera seed for the effective removal of these metal ions from real effluent. The maximum removal obtained was 85.29, 98.73, 97.55, 78.34, 65.45, 96.27, 89.64, 96.54 and 99.63% for Al, B, Cd, Cu, Fe, Mo, Ni, Pb and Zn species, respectively. On the other hand, concentration of Si and Mg species after adsorption process (12.33 and 0.0352 mg/l, respectively) was more than that of before adsorption process (3.34 and 0.0265, respectively), this may be due to dissolution of these species in the experimental condition. Fig. 26 shows that no target analytes were detected in the wastewater effluent by ICP, such as Co, Cr and V species, probably due to that fact they were below the detection limit (< 0.01 ppm).However, the results confirm that Moringa oleifera seeds are able to sufficiently remove different metal ions from real wastewater.

Table 5.Characterization of the raw wastewater.

Contaminants (ppm) by ICP instrument	EC (mg/L)	TDS (mg/L)	pH
Al(0.1441), B (0.0314), Cd (0.0245), Co ($1x10^{-3}$),Cr(0.0100),Cu(0.0277),Fe(0.1262), Mg (0.0265), Mo (0.0268), Ni (0.0193), Pb(0.2315), V(0.0100), Zn(0.1631), Si (3.3400)	512	307	7.56

REFERENCES

[1] M.A. Acheampong, J.P.C. Pereira, R.J.W. Meulepas, P.N.L.; Environ. Technol., 33 (4) (2012), 409-417,

[2] A. Zoghi, K. Khosravi-Darani, S. Sohrabvandi; Mini Rev. Med. Chem., 14 (2014), 84-98.

[3] D.Y. Lei, Z. Liu, Y.H. Peng, S.B. Liao, H. Xu; Ann. Microbiol., 64 (2014), 1371-1384.

[4] R. Amber, G. Federico, W.W. Leslie, M. Asli, P. Birgit; Vet. Med. Res. Rep., 4 (2013), 11-20.

[5] A.M.S. Vieira, M.F. Vieira, G.F. Silva, ÁA. Araújo, M.R. Fagundes-Klen, M.T. Veit, R.; Water Air Soil Pollut., 206 (1–4) (2010) 273-281,

[6] E. Arnoldsson, M. Bergam, N. Matsinhe, K.M.; J. Water Manag. Res., 64 (2008), 137-150.

[7] V. Nand, K. Koshy, M. Maata, S. Sotheeswaran; Int. J. Appl. Sci. Technol., 2 (2012), 125-129.

[8] C.S.T. Araújo, V.N. Alves, H.C. Rezende, L.S. Almeida, R.M.N. De Assunçâo, R. César, T. Tarley, M.G. Segatelli, N.M.M. Coelho; Water Science Technology 62 (2010) 2198-2203.

[9] H.M. Kwaambwa, R. Maikokera; Colloid Surf. B, 64 (2008), 118-125.

[10] N. Fenga, X.Guoa, S.Lianga; Journal of. Hazardous Materials164 (2009) 1286–1292.

[11] M. Tariq, A. I.Durrani, U. F., MadihaTariq; Journal of Environmental Management 223 (2018) 771-778.

[12] S.Tripathi, A. Roy, S. Nair, S.Durani, R. Bose; Environmental Nanotechnology, Monitoring & Management10**(**2018**)** 127-139.

[13] A. T. A.Baptista, M. O. Silva, R. G. Gomes, R.Bergamasco, M.F. Vieira, Angélica, M. S. Vieira; Separation and Purification Technology 180(2017) 114-124.

[14] T. G.Kebede, A. A,Mengistie, S.Dube, T..I..N.kambule, M. M.Nindi; Journal of Environmental Chemical Engineering 6 (2018) 1378-1389.

[15] K. Jayaram, M. N. V. Prasad; Journalof Hazardous Materials169 (2009)991-997.

[16] S. Fan, Y. Wang, Z. Wang, J. Tang, J. Tang, X. Lia; J. Environ. Chem. Eng, 5 (2017), 601-611.

[17] M.J.Ahmed, B.H.Hameed; Journal of Cleaner Production195(2018) 1162-1169.

[18] S.M. Abdulkarim, K. Long, O.M. Lai, S.K.S. Muhammad, H.M. Ghazali; Food Chemistry 93 (2005) 253-263.

[19] C.S.T. Araujo, D.C. Carvalho, H.C. Rezende, I.L.S. Almeida, L.M. Coelho, N.M.M. Coelho, T.L. Marques, V.N. Alves; Appl. Bioremediat. Act. Passiv.Approaches.InTech, 406 (2013)

[20] I. M.Reck, R. M.Paixão, R.Bergamasco, M. F. Vieira, A. M.S.Vieira; Journal of Cleaner Production171(2018) 85-97.

[21] M.A. Zazycki, M. Godinho, D. Perondi, E.L. Foletto, G.C. Collazzo, G.L. Dotto; Journal of Cleaner Production171 (2018), 57-65.

[22] M.Gan, Z. Song, S.Jie, J. Zhu, Y. Zhu, X. Liu; Materials Science and Engineering: C,59(2016) 990-997.

[23] G. A. P.Mateus, M.P.Paludo, T. R. T. Santos, M. F. Silva, R.Bergamasco; Journal of Environmental Chemical Engineering, 6,(2018), 4084-4092.

[24] T. G.Kebede, S.Dube, A. A.Mengistie, T.T.I.Nkambule, M. M.Nindi; Physics and Chemistry of the Earth Parts A/B/C Available online 8 August (2018)In Press,

[25] N.E. Nwaiwu, M.A. Zalkiful, I.A. Raufu; J. Appl. Phytotechnol. Environ. Sanit., 1 (2012), 1-9.

[26] H. M. Jang, S.Yoo, Y.Choi, S. Park,E.Kan;Bioresource Technology259(2018) 24-31.

[27] H. Zhang, X.Yue, F. Li, R. Xiao, D.Gu; Science of The Total Environment 631–632(2018) 795-802.

[28] W.Qian, X.Luo, X. Wang, M.Guo, B. Li; Ecotoxicology and Environmental Safety,157(2018) 300-306.

[29] A.B.Albadarin, M.N.Collins, M.Naushad, S.Shirazian, G. Walker, C.Mangwandi; Chemical Engineering Journal307 (2017) 264-272..

[30] B. BenguellaH Benaissa; Water Research36 (2002) 2463-2474.

[31] J.M. Santana-Caslano, M. Gonzalez-Davilla; Environmental Science Technolology 26 (1) (1992), 90-95.

[32] K. Anupam, S. Dutta, C. Bhattacharjee, S. Datta; Chemical Engineering Journal 173 (2011) 135-143.

[33] N. T.Cheng-Gang, N.Xue-Ting, L.C. Liang, H. G.Li-Shen, L.C.Zheng,G.Zeng; Science of The Total Environment 635(2018) 1331-1344.

[34] E.Alver, M.Bulut, A. Ü.Metin, H.Çiftçi; Spectro-chimical-Acta Part A: Molecular and

Biomolecular Spectroscopy 171 (2017) 132–138.

[35] L. Ding, H. Deng, C. Wu, X. Han; Chemical Engineering Journal181–182 (2012) 360-370.

[36] C.Jeon; Journal of Industrial and Engineering Chemistry 58 (2018) 57–63.

[37] S.Mukherjeea, S.Barmanb, G.Halder; Groundwater for Sustainable Development 7 (2018) 39–47.

[38] J. Jang, D. S. Lee; Science of the Total Environment 615 (2018) 549–557.

[39] T.Şahan, F.Erol, Ş.Yılmaz; Microchemical Journal 138 (2018) 360–368.

[40] M. A.Hanif, R.Nadeem, H. N.Bhatti, N. R. Ahmad, T. M. Ansari; Journal of Hazardous Materials139, (2007), 345-355.

[41] K.Y. Foo, B.H. Hameed; Chemical Engineering Journal, 156 (2010), 2-10.

[42] M.Luo, H. Lin,B.Li, Y.Dong, Y.He, L.Wang; Bioresource Technology259, (2018), 312-318.

[43] C.P.A.Silvaa, A. O. Jorgettoa, M. H.P. Wondracekb, R.M. G.,J.F. Schneiderc, M. J. Saekia, V.A. Pedrosaa, L.F. Zarad, G. R. Castroa; Groundwater for Sustainable Development 6 (2018) 50–56.

[44] J. Ray, S. Jana, T.Tripathy; International Journal of Biological Macromolecules 109 (2018) 492–506.

[45] S. Ben-AliImen, J.Souad, S.A.Ouederni; Journal of Cleaner Production142, Part 4, (2017), 3809-3821.

[46]I. Kara, D.Tunc, F.Sayin, S. T.Akar; Applied Clay Science, 161, (2018) 184-193.

[47] H.Zhouc, Z. Jiang.S.Weia; Applied Clay Science 153 (2018) 29–37.

[48] Singh, B., Das, S. K., Colloids and Surf. B: Biointer. 107 (2013) 97– 106.

[49] Anirudhan T.S., P.G. Radhakrishnan; J. Chem. Thermody., 40 (2008) 702–709.

[50] Sagnik C., Shamik Chowdhury, Papita Das Saha; Carbohyd. Polym. 86, (2011), 1533–1541.

[51] A. M.Nahum, E. Padilla-Ortega, C.R.María, R.Leyva-Ramos, R.Ocampo-Pérez, C. Carranza-Alvarez; Sustainable Environment Research, 27(2017) 61-69.

[52] J. Zhou, Y. Liu, X. Zhou, J. Ren, C. Zhong; Applied Surface Science, 427 (2018)976-985.

ملخص البحث

يوضح هذا العمل إحتمالية استخدام مسحوق بذور نبات المورينجا أوليفيرا كمادة مازة لإزالة المعادن الثقيلة من مياه الصرف الصحي، وقد تمت عملية دراسة الخصائص التركيبية المميزة لبودرة بذور المورينجا كمادة مازة لإزالة المعادن الثقيلة من مياه الصرف باستخدام تقنيات FTIR و XRD وpH_{pzc}و SEM و .BET.كما تمت دراسة العديد من العوامل المؤثرة على عملية المعالجة مثل؛ زمن النقع، جرعة المادة المازة، تركيزات أيونات الرصاص الأولية، ودرجة الحموضة، ودرجة الحرارة .تم تحليل بيانات التوازن الخاصة بعملية الامتزاز الحيوي باستخدام نماذج ايزوثيرمالية مثل Langmuirو Freundlich و Temkin و-Dubinin Radushkevichلتحديد أفضل نموذج لوصف عملية الامتزاز لإيونات الرصاص سواء كانت من المياه الملوثة الاصطناعية او الحقيقية، وقد وحد انهمن بين نماذج الايزوثيرم الأربعة، وجد ان كل من نموذج Temkinو Freundlich هما أفضل النماذج التى يمكن ان تصف عملية امتزاز ايون الرصاص، بشكل جيد بواسطة معامل التصحيح (R^2> 0.99).كما تبين انعملية الامتزاز تتبع النموزج الحركي ثنائى الرتبة.وقد فسرت عملية الازالة على ان التفاعل بين الأنواع الموجبة مع مسحوق بذور نبات المورينجا في الغالب عن طريق الامتزاز الكيميائي .كما تم تحديد العوامل الديناميكية الحرارية مثل: الطاقة الحرة، الانتروبى وحرارة التفاعل.